Editors' Suggestion | Featured in Physics

Controlling the Shape of Small Clusters with and without Macroscopic Fields

Francesco Boccardo* and Olivier Pierre-Louis†
Institut Lumière Matière, UMR5306 Université Lyon 1—CNRS, 69622 Villeurbanne, France

(Received 30 November 2021; accepted 9 May 2022; published 22 June 2022)

Despite major advances in the understanding of the formation and dynamics of nanoclusters in the past decades, theoretical bases for the control of their shape are still lacking. We investigate strategies for driving fluctuating few-particle clusters to an arbitrary target shape in minimum time with or without an external field. This question is recast into a first passage problem, solved numerically, and discussed within a high temperature expansion. Without field, large-enough low-energy target shapes exhibit an optimal temperature at which they are reached in minimum time. We then compute the optimal way to set an external field to minimize the time to reach the target, leading to a gain of time that grows when increasing cluster size or decreasing temperature. This gain can shift the optimal temperature or even create one. Our results could apply to clusters of atoms at equilibrium, and colloidal or nanoparticle clusters under thermo- or electrophoresis.

DOI: 10.1103/PhysRevLett.128.256102

Less than a decade after its discovery [1], scanning tunneling microscopy was used to position atoms on a surface with Ånsgtrom precision [2], reaching atomic-scale control on the organization of matter. Following this seminal work, many examples of organization of atoms [3,4], molecules or nanoparticles [5–9], and colloids [10,11] were obtained with tools like scanning tunneling microscopy, atomic force microscopy, or optical tweezers. However, important challenges are still open in the control of few-particle clusters.

The first one is to control matter at the nanoscale with an external macroscopic field that does not act on one single particle or atom at a time, but on the whole cluster. External fields such as light acting on metal nanoparticle clusters [12] or electromigration acting on atomic monolayer clusters [13–16] are known to lead to complex equilibrium or nonequilibrium cluster shapes. However, these shapes are only a very small fraction of all possible shapes, which are dictated by the physics of the interaction of the driving force with the system.

Another challenge lies in the ability to obtain refined control of nanostructure shapes in the presence of thermal fluctuations that activate the random diffusion of particles and atoms, leading to shape fluctuations [15,17,18]. Some progress in this direction has been achieved with the control of the formation and order of colloidal clusters [19–21] in finite-temperature experiments. However, the control of the cluster shape is still an open issue.

In order to address these challenges, we investigate strategies to reach arbitrary cluster shapes in minimum time in the presence of fluctuations. We focus on the control of few-particle two-dimensional clusters and find how a given target shape can be reached in minimum time with and without macroscopic external field. This problem, which is formulated as the minimization of a first passage time on the graph of cluster configurations, is solved numerically and studied analytically with the help of a high temperature expansion.

In the absence of field, we find that large compact target shapes exhibit an optimal temperature at which they can be reached in minimum time. In the presence of an external field we use dynamic programming [22,23] to find the optimal way to set the external field as a function of the cluster shape to reach the target in minimum time. The gain in time due to the forces increases with decreasing temperature and with increasing clusters size. This gain can shift the optimal temperature, or create one when it does not exist in the absence of forces.

We focus on clusters with edge diffusion dynamics. Edge diffusion was observed in metal atomic monolayer islands [24,25], and for colloids [26]. However, our strategy can readily be extended to any type of dynamics that preserves the number of particles such as surface-diffusion dynamics inside vacancy clusters [27–29], or dislocation-mediated cluster rearrangements in colloids [30] and metal nanoclusters [31,32]. We discuss possible experiments with clusters of atoms or colloids.

Model.—We consider a small cluster on a square lattice with lattice parameter a and nearest-neighbor bonds J under an external macroscopic force $\boldsymbol{F}$. We assume that the current configuration of the cluster, hereafter denoted as the state s, can be observed at all times. The force is chosen as a function of s. This choice is encoded in the policy $\boldsymbol{\phi}$, so that $\boldsymbol{F} = \boldsymbol{\phi}(s)$. The state s can change to another state s' via the motion of a single particle to one of its nearest or next-nearest neighbor sites along the cluster edge. Moves that break the cluster are forbidden. Following usual models for biased diffusion

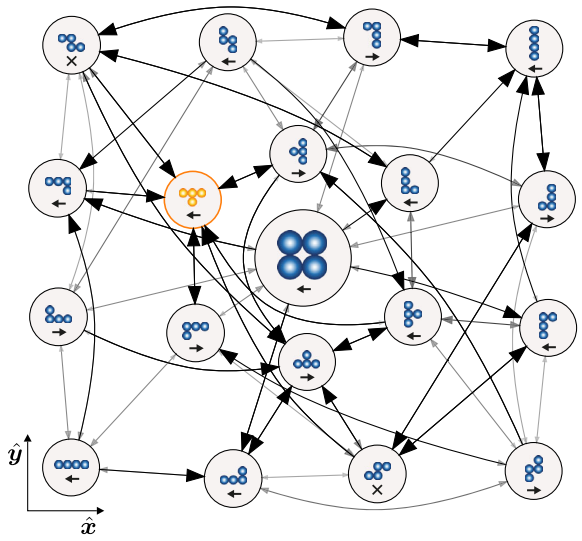

FIG. 1. Graph of configurations for a tetramer cluster ($N = 4$) at $T = 0.24$. The node size is proportional to the expected residence time $t_{\boldsymbol{\phi}}(s)$. The thickness and shade of the edges are proportional to the transition probability $p_{\boldsymbol{\phi}}(s, s')$. Arrows in the nodes represent an optimal policy $\boldsymbol{\phi}_*(s)$ to reach the orange target shape (crosses correspond to a zero force).

[15,33,34], the hopping rate is assumed to take an Arrhenius form

$$\gamma_{\boldsymbol{\phi}}(s, s') = \nu \exp\{-[n_{ss'}J - \boldsymbol{\phi}(s) \cdot \boldsymbol{u}_{ss'}]/k_B T\}, \quad (1)$$

where $k_B T$ is the thermal energy and ν is an attempt frequency, $n_{ss'}$ is the number of in-plane nearest neighbors in state s before hopping. To gain computation time, we freeze atoms with $n_{ss'} = 4$. In addition, we assume that the displacement vector to the diffusion saddle point $\boldsymbol{u}_{ss'}$ is half the displacement vector between the initial and final positions of the moving atom [15]. In the following, we choose units where $k_B = 1$, $J = 1$, $\nu = 1$, and $a = 1$.

Our goal is to study the time to reach a target cluster configuration $\bar{s}$ from an initial state s. This time can be seen as a first passage time $\tau_{\boldsymbol{\phi}}(s, \bar{s})$ in a random walk on the graph of cluster configurations [35,36], as represented in Fig. 1. Since the dynamics is Markovian, $\tau_{\boldsymbol{\phi}}(s, \bar{s})$ is equal to the expected residence time $t_{\boldsymbol{\phi}}(s)$ in state s plus the first passage time from the new state s' after the move [37]. Considering all possible moves, we obtain a recursion relation

$$\tau_{\boldsymbol{\phi}}(s, \bar{s}) = t_{\boldsymbol{\phi}}(s) + \sum_{s' \in \mathcal{B}_s} p_{\boldsymbol{\phi}}(s, s') \tau_{\boldsymbol{\phi}}(s', \bar{s}), \quad (2)$$

where $p_{\boldsymbol{\phi}}(s, s') = \gamma_{\boldsymbol{\phi}}(s, s') t_{\boldsymbol{\phi}}(s)$ is the transition probability from s to s', $t_{\boldsymbol{\phi}}(s) = 1/\sum_{s' \in \mathcal{B}_s} \gamma_{\boldsymbol{\phi}}(s, s')$, and $\mathcal{B}_s$ the set of states that can be reached from s via a single move.

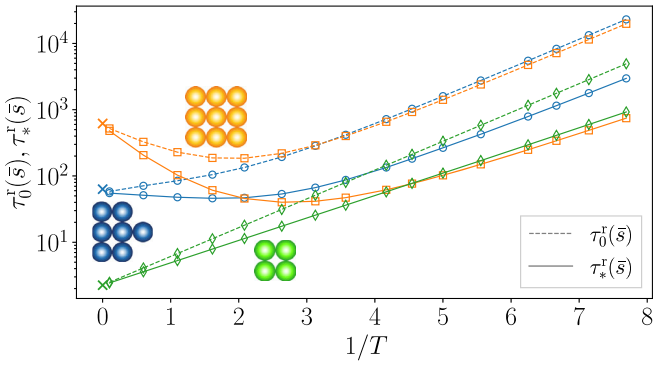

FIG. 2. Expected return time to target as a function of $1/T$. Zero-force case $\tau_0^r(\bar{s})$ and under the optimal policy $\tau_*^r(\bar{s})$ with $F_0 = 0.4$. The $\times$ corresponds to $\tau_\infty^r(\bar{s})$ for $T \to \infty$.

Relation Eq. (2) is supplemented with the boundary condition $\tau_{\boldsymbol{\phi}}(\bar{s}, \bar{s}) = 0$.

We also define the expected return time to target, i.e., spent outside the target before returning to it when starting from the target itself [38]

$$\tau_{\boldsymbol{\phi}}^r(\bar{s}) = \sum_{s \in \mathcal{B}_{\bar{s}}} p_{\boldsymbol{\phi}}(\bar{s}, s) \tau_{\boldsymbol{\phi}}(s, \bar{s}). \quad (3)$$

For the sake of concision, we mainly focus on the analysis of $\tau_{\boldsymbol{\phi}}^r(\bar{s})$ instead of $\tau_{\boldsymbol{\phi}}(s, \bar{s})$ which is different for each s.

Zero force.—Let us first set the force to zero in all states, $\boldsymbol{\phi}(s) = \mathbf{0}$. This leads to standard equilibrium fluctuation dynamics that have been investigated thoroughly in the case of edge diffusion [17,18,24]. Although some quantities related to first passage processes have been discussed within the frame of persistence of fluctuations [39,40], there is to our knowledge no study of the first passage times to cluster configurations. We have evaluated $\tau_{\boldsymbol{\phi}}(s, \bar{s})$ numerically using the method of iterative evaluation [22]: for a given $\bar{s}$, we iterate the evaluation of $\tau_{\boldsymbol{\phi}}(s, \bar{s})$ by substitution of its value in the right-hand side of Eq. (2). Since it requires to list all states, such a method is suitable for small clusters, which corresponds to our focus in this Letter. Indeed, the total number S_N of configurations for a cluster with N particles, often called polyominoes or lattice animals [41], grows exponentially with N: $S_N \sim c\lambda^N/N$, with $\lambda \approx 4.0626$ and $c \approx 0.3169$ [42]. We have performed simulations with $N \leq 12$, with $S_{12} \approx 5 \times 10^5$ states.

The resulting expected return time to target with zero force $\tau_0^{\mathrm{r}}(\bar{s})$ is shown in Fig. 2 as a function of $1/T$. For small clusters, $\tau_0^{\mathrm{r}}(\bar{s})$ increases monotonically as the temperature is decreased. This is expected because thermally activated hopping diffusion events become slower at low temperatures. However, $\tau_0^{\mathrm{r}}(\bar{s})$ exhibits a minimum as a function of temperature for clusters that are larger and more compact. As shown in the Supplemental Material [43], a similar minimum is found in the time $\tau_0(s, \bar{s})$ to reach the target starting from any state s. This striking result implies

that some targets exhibit an optimal temperature at which the target can be reached in minimum time.

The presence of a minimum is associated to a change of slope of $\tau_0^{\mathrm{r}}(\bar{s})$ as a function of $1/T$ at high temperatures. We therefore study the high temperature behavior in more detail. In the limit $T \to \infty$, the rates (1) are independent of the initial and final state and of the force: $\gamma_{\boldsymbol{\phi}}(s,s') \to 1$. As a consequence, $\tau_{\boldsymbol{\phi}}^{\mathrm{r}}(\bar{s})$ is independent of the policy $\boldsymbol{\phi}$ at infinite temperature $\tau_{\boldsymbol{\phi}}^{\mathrm{r}}(\bar{s}) \to \tau_\infty^{\mathrm{r}}(\bar{s})$. A simple result is known from the literature [44] (see also Supplemental Material [43]) when all rates are equal: $\tau_\infty^{\mathrm{r}}(\bar{s}) = (S_N - 1)/d_{\bar{s}}$, where the degree $d_{\bar{s}}$ of the target is the number of states that can be reached from the target $\bar{s}$ in one move. This quantity is similar to the lower bound of the mean first passage time (averaged over all initial states s), which is often used to characterize first passages in random graphs [45–48].

When the temperature is decreased, the moves become sensitive to the energy. From detailed balance, a move that leads to a decrease of energy is faster than the reverse move. As a consequence, the cluster goes faster towards states with lower energy. Thus, the time to reach the target decreases if the target has a lower energy. However, this trend is only describing relative variations of the time to reach different targets. When decreasing the temperature, there is also a global slowing-down of the dynamics because of the Arrhenius dependence of the rates on temperature in Eq. (1). The decrease or increase of first passage times to the target—or equivalently of $\tau_{\boldsymbol{\phi}}^{\mathrm{r}}(\bar{s})$—depends on the competition between these two effects: relative energy effect vs global slowing down.

This competition can be analyzed from a high temperature expansion to first order in $1/T$ (details are reported in the Supplemental Material [43]), leading to

$$\tau_0^r(\bar{s}) = \left(1 + \frac{M_0(\bar{s})}{T}\right)\tau_\infty^r(\bar{s}), \tag{4}$$

$$M_0(\bar{s}) = \frac{1}{1 - S_N^{-1}}\langle \tilde{\delta}_{s\bar{s}} \langle n_{ss'}\rangle_{s'} - d_s g_n(s,\bar{s})\rangle_{s\in\mathcal{S}}, \tag{5}$$

where $\tilde{\delta}_{ss'} = 1 - \delta_{ss'}$ with δ the Kronecker symbol, $\langle\cdot\rangle_{s\in\mathcal{Z}}$ indicates the average over the states in the set of states $\mathcal{Z}$, and $\mathcal{S}$ is the set of all states. We also use the notation $\langle\cdot\rangle_{s'} = \langle\cdot\rangle_{s'\in\mathcal{B}_s}$. In addition, the local covariance of any quantity $q_{ss'}$ with $\tau_\infty(s,\bar{s})$ is defined as

$$g_q(s,\bar{s}) = \langle (q_{ss'} - \langle q_{ss''}\rangle_{s''})(\tau_\infty(s',\bar{s}) - \langle \tau_\infty(s'',\bar{s})\rangle_{s''})\rangle_{s'},$$

where $\langle\cdot\rangle_{s''} = \langle\cdot\rangle_{s''\in\mathcal{B}_s}$. In Fig. 3(a), we see that Eq. (5) is in good agreement with the value $M_0^{\mathrm{sim}}(\bar{s})$ obtained from a high temperature fit of the numerical solution from iterative evaluation (small deviations are caused by the freezing of 4-neighbor particles).

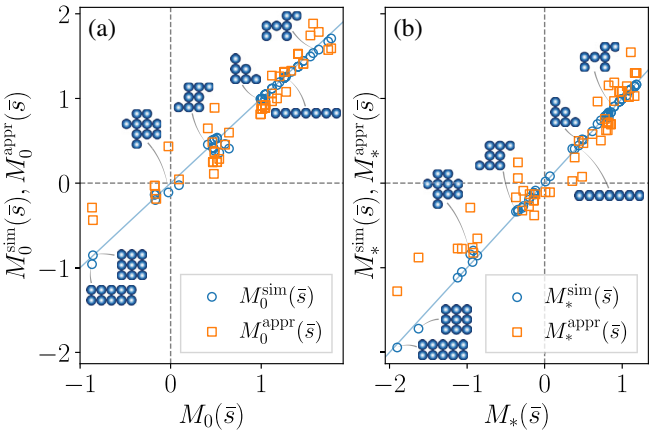

FIG. 3. Estimates of the high temperature slope. $M_0(\bar{s})$ and $M_*(\bar{s})$ correspond to the analytical expressions of Eqs. (5),(8). $M_0^{\mathrm{sim}}(\bar{s})$ and $M_*^{\mathrm{sim}}(\bar{s})$ are the slopes extracted from a high temperature fit using iterative numerical methods. $M_0^{\mathrm{appr}}(\bar{s})$ and $M_*^{\mathrm{appr}}(\bar{s})$ are approximate expressions from Eqs. (6), and (9).

In Eq. (5), the first term proportional to $\langle n_{ss'}\rangle_{s'}$ accounts for the global slowing down of the dynamics, while the second term proportional to $d_s g_n(s,\bar{s})$ accounts for the relative energy effect. The global slowing down contribution can be approximated by $\rho_0(N) = \langle\langle n_{ss'}\rangle_{s'}\rangle_{s\in\mathcal{S}}$, which converges exponentially to $\rho_0(\infty) \approx 1.64$ for large N (see Supplemental Material [43] for details). The relative energy effect is dominated by moves from $\mathcal{B}_{\bar{s}}$ to the target. It is approximately proportional to a measure of cluster compactness defined as the difference in the number of bonds to break between moves leading to and moves not leading to the target $\langle n_{s\bar{s}} - \langle n_{ss''}\rangle_{s''}\rangle_-$, where $\langle\cdot\rangle_- = \langle\cdot\rangle_{s\in\mathcal{B}_{\bar{s}}}$. This relation is derived and checked in the Supplemental Material [43]. We therefore obtain

$$M_0^{\mathrm{appr}}(\bar{s}) = \rho_0(N) + \rho_1\langle n_{s\bar{s}} - \langle n_{ss''}\rangle_{s''}\rangle_-, \tag{6}$$

where $\rho_1 \approx 1.60$. As shown in Fig. 3(a), $M_0^{\mathrm{appr}}(\bar{s})$ provides a fair approximation to $M_0(\bar{s})$. The dispersion originates from assumptions of uncorrelation of τ_∞ with $n_{ss'}$, and of variations of τ_∞ dominated by the difference between $\tau_\infty(\bar{s},\bar{s}) = 0$ on the target and $\tau_\infty(s,\bar{s})$ in its neighborhood $\mathcal{B}_{\bar{s}}$. The sign of $M_0^{\mathrm{appr}}(\bar{s})$ can serve as a simple guide to the presence of a minimum as a function of T, i.e., an optimal temperature, and also makes explicit the link between the minimum and the compactness of the target. For example, in a linear one-atom-thick target, only the two atoms at the tips can move, so that $\langle n_{s\bar{s}}\rangle_- = 1$ and an inspection of the possible moves shows that $\langle\langle n_{ss''}\rangle_{s''}\rangle_- = 4/3$. This leads to $M_0^{\mathrm{appr}}(\bar{s}) = \rho_0(N) - \rho_1/3 \approx 0.9 > 0$ for $N = 7$, in agreement with $M_0^{\mathrm{sim}}(\bar{s}) \approx 1.04$ found by iterative evaluation. In contrast, in the limit of large compact (square, rectangular, etc) islands, for which $\langle n_{s\bar{s}}\rangle_- = 1$ and $\langle\langle n_{ss''}\rangle_{s''}\rangle_- \to 3$, we obtain $M_0^{\mathrm{appr}}(\bar{s}) = -1.57 < 0$ leading to a minimum.

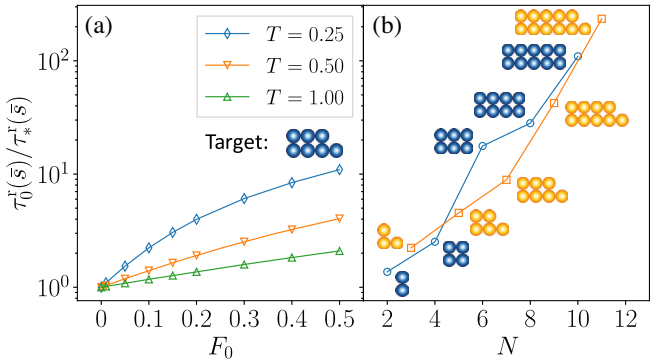

FIG. 4. Gain $\tau_0^r(\bar{s})/\tau_*^r(\bar{s})$ in the return time to target due to the optimization of the forces. (a) As a function of the force magnitude F_0, for a fixed target at different T. (b) For similar targets of increasing size, with $T = 0.24$ and $F_0 = 0.4$.

Note, however, that the convergence of value iteration is difficult not only for large clusters, but also for high-energy (i.e., noncompact) target shapes when the temperature is decreased. Indeed, disparate timescales have to be resolved (fast relaxation towards low-energy shapes vs large time to reach high-energy shapes).

Optimal policy in the presence of forces.—Our goal now is to determine the optimal policy $\boldsymbol{\phi}_*$ that minimizes $\tau_{\boldsymbol{\phi}}(s)$, and the resulting optimal first passage time $\tau_*(s,\bar{s}) = \min_{\boldsymbol{\phi}} \tau_{\boldsymbol{\phi}}(s,\bar{s})$ for nonzero forces. Such a problem, called a Markov decision process, can be solved using well-known dynamic programming methods [22,23]. We substitute the optimal policy in Eq. (2) to obtain the so-called Bellmann optimality equation

$$\tau_*(s,\bar{s}) = \min_{\boldsymbol{\phi}(s)} \left[t_{\boldsymbol{\phi}}(s) + \sum_{s' \in \mathcal{B}_s} p_{\boldsymbol{\phi}}(s,s') \tau_*(s',\bar{s}) \right]. \quad (7)$$

As in the zero-force case, we iterate Eq. (7). However minimization over the force in s is taken at each iteration. This method, called value iteration, provides both $\tau_*(s,\bar{s})$ and the optimal policy $\boldsymbol{\phi}_*$. Because of the fast increase of S_N with N, its computational cost grows exponentially with N (see Supplemental Material [43]).

We choose a force $\boldsymbol{F}$ that is always oriented in $\hat{\boldsymbol{x}}$ direction [(10) lattice direction], with 3 possible values: $\{-F_0\hat{\boldsymbol{x}}, \boldsymbol{0}, F_0\hat{\boldsymbol{x}}\}$, with $F_0 > 0$. An example of optimal policy is shown in Fig. 1. As an important remark, the force can drive the cluster towards any target shape even if the symmetries of the target are not compatible with those of the force because observation itself (i.e., the knowledge of s) breaks the symmetry.

The gain due to the optimal policy is reported in Fig. 4, using the zero-force policy as a reference. In the Supplemental Material [43], we show that using a random-force policy as a reference leads to similar results. As seen from Fig. 4(a), the gain increases not only when F_0 is increased, but also when T is decreased. This is intuitively expected since the relative change between different rates due to a change of the force increases when F_0/T is increased. In addition, the gain increases when the size of the cluster increases, as shown in Fig. 4(b). A naive explanation for this trend is that an increase of N leads to an increase of the number of states S_N, and therefore to an increase of the number of ways to tune the policy $\boldsymbol{\phi}$ in order to minimize $\tau_{\boldsymbol{\phi}}(s,\bar{s})$.

Again, a high temperature expansion leads to (derivation reported in the Supplemental Material [43])

$$\tau_*^r(\bar{s}) = \left(1 + \frac{M_*(\bar{s})}{T}\right) \tau_\infty^r(\bar{s}),$$
$$M_*(\bar{s}) = M_0(\bar{s}) - \frac{F_0}{1 - S_N^{-1}} \langle |\tilde{\delta}_{s\bar{s}} \langle u_{ss'} \rangle_{s'} - d_s g_u(s,\bar{s})| \rangle_{s \in \mathcal{S}}, \quad (8)$$

where $u_{ss'} = \boldsymbol{u}_{ss'} \cdot \hat{\boldsymbol{x}}$. The numerical solution of Eq. (7) is in agreement with Eq. (8) (up to small deviations due to four-neighbor particle freezing, see the Supplemental Material [43]).

Two remarks are in order. First, $\langle u_{ss'} \rangle_{s'}$ is small and its contribution to the term proportional to F_0 in Eq. (8) is negligible. Second, the absolute value forbids the cancellation of contributions with randomly different signs, leading to a behavior that is qualitatively different from that of $M_0(\bar{s})$. Indeed, the average is not dominated by the largest terms coming from the strong change of $\tau_\infty(s,\bar{s})$ between the target and its first neighbors, but by the typical values of $|d_s g_u(s,\bar{s})|$ in all states. Based on this observation, a detailed analysis reported in the Supplemental Material [43] leads to the approximation

$$M_*^{\text{appr}}(\bar{s}) = M_0(\bar{s}) - \frac{2^{1/2}}{\pi^{1/2}} F_0 \sigma_u \sigma_{\tau_\infty}(\bar{s}) \langle d_s^{1/2} \rangle_{s \in \mathcal{S}}, \quad (9)$$

where we have defined the standard deviations

$$\sigma_u = \langle \langle (u_{ss'} - \langle u_{ss''} \rangle_{s''})^2 \rangle_{s'}^{1/2} \rangle_{s \in \mathcal{S}}, \quad (10)$$

$$\sigma_{\tau_\infty}(\bar{s}) = \langle \langle (\tau_\infty(s',\bar{s}) - \langle \tau_\infty(s'',\bar{s}) \rangle_{s''})^2 \rangle_{s'}^{1/2} \rangle_{s \in \mathcal{S}}. \quad (11)$$

In Fig. 3, the approximation Eq. (9) is seen to be valid up to some dispersion originating mainly in the assumption of uncorrelation between $u_{ss'}$ and τ_∞.

While $\langle n_{s\bar{s}} - \langle n_{ss''} \rangle_{s''} \rangle_-$ and σ_u are bounded because $1 \le n_{ss'} \le 4$ and $-1/2 \le -u_{ss'} \le 1/2$, the quantities $\sigma_{\tau_\infty}(\bar{s})$ and $\langle d_s^{1/2} \rangle_{s \in \mathcal{S}}$ grow with N (see Supplemental Material [43]). Hence, from Eq. (6), $M_0^{\text{appr}}(\bar{s})$ is bounded and the contribution proportional to F_0 in Eq. (9) usually dominates over the term $M_0(\bar{s})$ for large N. Thus, when N is large enough, $M_*(\bar{s})$ should be negative and an optimal temperature should be generically present. This trend is confirmed by Fig. 3(b). Simulations with $N = 12$ and $F_0 = 0.4$

(reported in Fig. 10 of the Supplemental Material [43]) also confirm the generic presence of a minimum for larger targets.

Discussion.—For atomic metals clusters where edge diffusion is observed (Ag, Cu, etc.), estimates of the edge diffusion barrier $\sim J$ or kink energies $\sim J/2$ suggest that $J \approx 0.2$ to 0.3 eV [24,49–52]. For the square 9-atom target depicted in Fig. 2 the optimal temperature corresponds to $J/k_BT \approx 2$. Choosing $J = 0.2$ eV we obtain an optimal temperature $\approx 10^3$ K which is too high to be observed in usual experiments. Thus, $\tau_0(s, \bar{s})$ should decrease with temperature in usual experimental conditions. If needed, a quench can also be used to freeze the cluster once the target shape is reached. However, using electromigration as an external force leads to [25] $F_0 a/J \approx 10^{-4}$, which is too small to allow for the control of few-atom clusters.

Edge diffusion can also be observed with colloids [26]. Using colloids with depletants, $J\sim$ few k_BT [53]. The optimal temperature should then be observable in the absence of force. Thermophoretic forces [54–56] for polystyrene beads of radius 2.5 μm are $\sim 10\ k_BT/\mu$m [54]. Hence, micron-size colloids can lead to $F_0 a/J \sim 1$, which allows for shape control by a macroscopic force.

However, most experiments on colloid clusters report mass transport dominated by attachment-detachment at the edges [57]. Our analysis can be adapted to vacancy clusters [5,58,59] with volume-preserving detachment-diffusion-reattachment events. Moreover, other two- or three-dimensional lattices also could be analyzed. Furthermore, multiparticle and off-lattice processes (such as those involved in dislocation-mediated dynamics) can be included as long as they are predetermined (using, e.g., energy-exploration methods) and their number is finite, to allow for the numerical solution of Eqs. (2) and (7). Since the presence of the minimum depends only on the generic competition between the relative energy effect and global slowing down, we speculate that it should not depend on the details of mass transport kinetics.

In conclusion, thermal fluctuations can be used to reach desired nanocluster shapes. There is a temperature that minimizes the time to reach large-enough and compact shapes. Furthermore, macroscopic fields can help gaining orders of magnitude in the time to reach arbitrary shapes. We hope that our Letter will motivate experimental investigations for the control of atomic and colloidal clusters, and will open theoretical directions for the optimization of first passage times on graphs.

*francesco.boccardo@univ-lyon1.fr
†olivier.pierre-louis@univ-lyon1.fr

[1] G. Binnig and H. Rohrer, Surf. Sci. **126**, 236 (1983).
[2] D. M. Eigler and E. K. Schweizer, Nature (London) **344**, 524 (1990).
[3] A. Cooper, J. P. Covey, I. S. Madjarov, S. G. Porsev, M. S. Safronova, and M. Endres, Phys. Rev. X **8**, 041055 (2018).
[4] D. Barredo, S. de Léséleuc, V. Lienhard, T. Lahaye, and A. Browaeys, Science **354**, 1021 (2016).
[5] A. Martínez-Galera, I. Brihuega, A. Gutiérrez-Rubio, T. Stauber, and J. Gómez-Rodríguez, Sci. Rep. **4**, 1 (2014).
[6] D. Erickson, X. Serey, Y.-F. Chen, and S. Mandal, Lab Chip **11**, 995 (2011).
[7] T. Junno, K. Deppert, L. Montelius, and L. Samuelson, Appl. Phys. Lett. **66**, 3627 (1995).
[8] C. Baur, A. Bugacov, B. E. Koel, A. Madhukar, N. Montoya, T. R. Ramachandran, A. A. G. Requicha, R. Resch, and P. Will, Nanotechnology **9**, 360 (1998).
[9] F. J. Rubio-Sierra, W. M. Heckl, and R. W. Stark, Adv. Eng. Mater. **7**, 193 (2005).
[10] P. T. Korda, M. B. Taylor, and D. G. Grier, Phys. Rev. Lett. **89**, 128301 (2002).
[11] D. G. Grier, Nature (London) **424**, 810 (2003).
[12] P. McCormack, F. Han, and Z. Yan, J. Phys. Chem. Lett. **9**, 545 (2018).
[13] P. Kuhn, J. Krug, F. Hausser, and A. Voigt, Phys. Rev. Lett. **94**, 166105 (2005).
[14] M. Mahadevan and R. M. Bradley, Phys. Rev. B **59**, 11037 (1999).
[15] O. Pierre-Louis and T. L. Einstein, Phys. Rev. B **62**, 13697 (2000).
[16] S. Curiotto, F. Leroy, P. Müller, F. Cheynis, M. Michailov, A. El-Barraj, and B. Ranguelov, J. Cryst. Growth **520**, 42 (2019).
[17] S. V. Khare, N. C. Bartelt, and T. L. Einstein, Phys. Rev. Lett. **75**, 2148 (1995).
[18] K. C. Lai, D.-J. Liu, and J. W. Evans, Phys. Rev. B **96**, 235406 (2017).
[19] J. J. Juárez and M. A. Bevan, Adv. Funct. Mater. **22**, 3833 (2012).
[20] J. J. Juárez, P. P. Mathai, J. A. Liddle, and M. A. Bevan, Lab Chip **12**, 4063 (2012).
[21] Y. Xue, D. J. Beltran-Villegas, X. Tang, M. A. Bevan, and M. A. Grover, IEEE Trans. Control Syst. Technol. **22**, 1956 (2014).
[22] R. S. Sutton and A. G. Barto, *Reinforcement Learning: An Introduction*, 2nd ed. (The MIT Press, Cambridge, MA, 2018).
[23] R. E. Bellman, *Dynamic Programming* (Dover Publications, Inc., USA, 2003).
[24] M. Giesen, Prog. Surf. Sci. **68**, 1 (2001).
[25] C. Tao, W. G. Cullen, and E. D. Williams, Science **328**, 736 (2010).
[26] B. C. Hubartt and J. G. Amar, J. Chem. Phys. **142**, 024709 (2015).
[27] R. Plass, J. A. Last, N. Bartelt, and G. Kellogg, Nature (London) **412**, 875 (2001).
[28] J. Heinonen, I. Koponen, J. Merikoski, and T. Ala-Nissila, Phys. Rev. Lett. **82**, 2733 (1999).
[29] F. Leroy, A. El Barraj, F. Cheynis, P. Müller, and S. Curiotto, Phys. Rev. B **102**, 235412 (2020).
[30] B. VanSaders and S. C. Glotzer, Proc. Natl. Acad. Sci. U.S.A. **118**, e2017377118 (2021).
[31] R. Huang, Y. Wen, A. F. Voter, and D. Perez, Phys. Rev. Mater. **2**, 126002 (2018).

[32] O. Trushin, P. Salo, M. Alatalo, and T. Ala-Nissila, Surf. Sci. **482–485**, 365 (2001).
[33] S. Glasstone, K. J. Laidler, and H. Eyring, *The Theory of Rate Processes: The Kinetics of Chemical Reactions, Viscosity, Diffusion and Electrochemical Phenomena*, International chemical series (McGraw-Hill Book Company, Inc., New York, 1941).
[34] D.-J. Liu and J. D. Weeks, Phys. Rev. B **57**, 14891 (1998).
[35] J. R. Sanchez and J. W. Evans, Phys. Rev. B **59**, 3224 (1999).
[36] N. Combe and H. Larralde, Phys. Rev. B **62**, 16074 (2000).
[37] N. G. Van Kampen, *Stochastic Processes in Physics and Chemistry* (Elsevier, New York, 1992).
[38] As a technical remark, this definition requires to extend the policy and define a force on the target state itself. However, due to the Markovian character of the dynamics, this does not affect the mean first passage time to target and the optimal policy in the other states outside the target.
[39] D. B. Dougherty, I. Lyubinetsky, E. D. Williams, M. Constantin, C. Dasgupta, and S. Das Sarma, Phys. Rev. Lett. **89**, 136102 (2002).
[40] M. Constantin, S. Das Sarma, C. Dasgupta, O. Bondarchuk, D. B. Dougherty, and E. D. Williams, Phys. Rev. Lett. **91**, 086103 (2003).
[41] A. J. Guttmann, *Polygons, Polyominoes and Polycubes*, Lecture Notes in Physics 775 (Springer, New York, 2009).
[42] I. Jensen and A. J. Guttmann, J. Phys. A: Math. Theor. **33**, L257 (2000).
[43] See Supplemental Material at http://link.aps.org/supplemental/10.1103/PhysRevLett.128.256102 for details about: (i) expected return time to target vs time to target from other states, (ii) high temperature expansion of the expected return time to target, (iii) zero-force vs random policy, (iv) optimal return time to target for big targets, (v) computation time as a function of cluster size, and (vi) effect of freezing atoms with 4 nearest neighbors.
[44] L. Lovász, Combinatorics, Paul erdos is eighty **2**, 4 (1993).
[45] Y. Lin, A. Julaiti, and Z. Zhang, J. Chem. Phys. **137**, 124104 (2012).
[46] V. Tejedor, O. Bénichou, and R. Voituriez, Phys. Rev. E **80**, 065104(r) (2009).
[47] A. Baronchelli and V. Loreto, Phys. Rev. E **73**, 026103 (2006).
[48] J. D. Noh and H. Rieger, Phys. Rev. Lett. **92**, 118701 (2004).
[49] R. Ferrando and G. Tréglia, Phys. Rev. B **50**, 12104 (1994).
[50] B. D. Yu and M. Scheffler, Phys. Rev. B **55**, 13916 (1997).
[51] H. Mehl, O. Biham, I. Furman, and M. Karimi, Phys. Rev. B **60**, 2106 (1999).
[52] R. Nelson, T. Einstein, S. Khare, and P. Rous, Surf. Sci. **295**, 462 (1993).
[53] J. Nozawa, S. Uda, S. Guo, A. Toyotama, J. Yamanaka, N. Ihara, and J. Okada, Cryst. Growth Des. **18**, 6078 (2018).
[54] L. Helden, R. Eichhorn, and C. Bechinger, Soft Matter **11**, 2379 (2015).
[55] M. Braibanti, D. Vigolo, and R. Piazza, Phys. Rev. Lett. **100**, 108303 (2008).
[56] A. Würger, Rep. Prog. Phys. **73**, 126601 (2010).
[57] R. Ganapathy, M. R. Buckley, S. J. Gerbode, and I. Cohen, Science **327**, 445 (2010).
[58] P. García, R. Sapienza, A. Blanco, and C. López, Adv. Mater. **19**, 2597 (2007).
[59] J. A. Pariente, N. Caselli, C. Pecharromn, A. Blanco, and C. López, Small **16**, 2002735 (2020).